Supplementary Information

Enhanced ionic conductivity and chemical stability of anion exchange membrane prepared from ether-free poly(biphenyl alkylene piperidinium) with alkyl spacer for water electrolysis

*Thi Cam Thach To, Anh Le Mong, and Dukjoon Kim**

T.C.T. To, A.L. Mong, Prof. D. Kim

School of Chemical Engineering, Sungkyunkwan University, Gyeonggi, Suwon, 16419, Republic of Korea.

E-mail: djkim@skku.edu

Number of figures: 10

Number of pages: 18

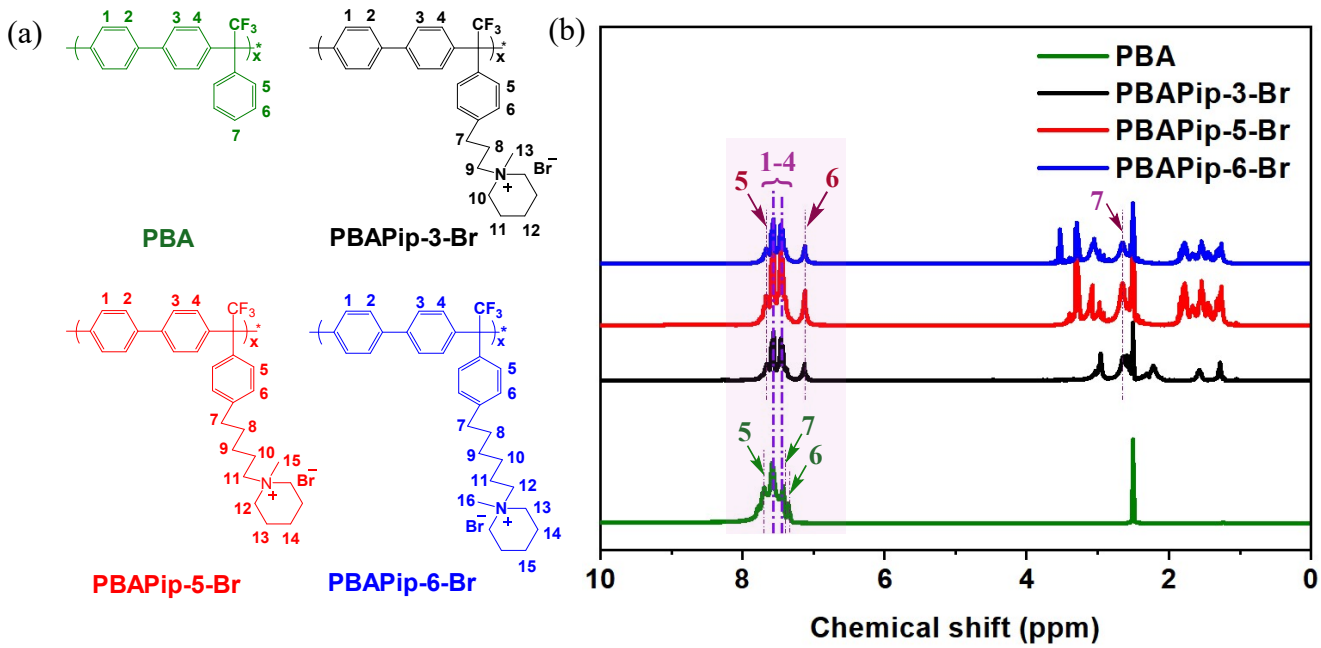

Figure S1. (a) Chemical structures; and (b) ^{1}H-NMR spectra of PBA and PBAPip-n-Br membranes (n = 3, 5, and 6).

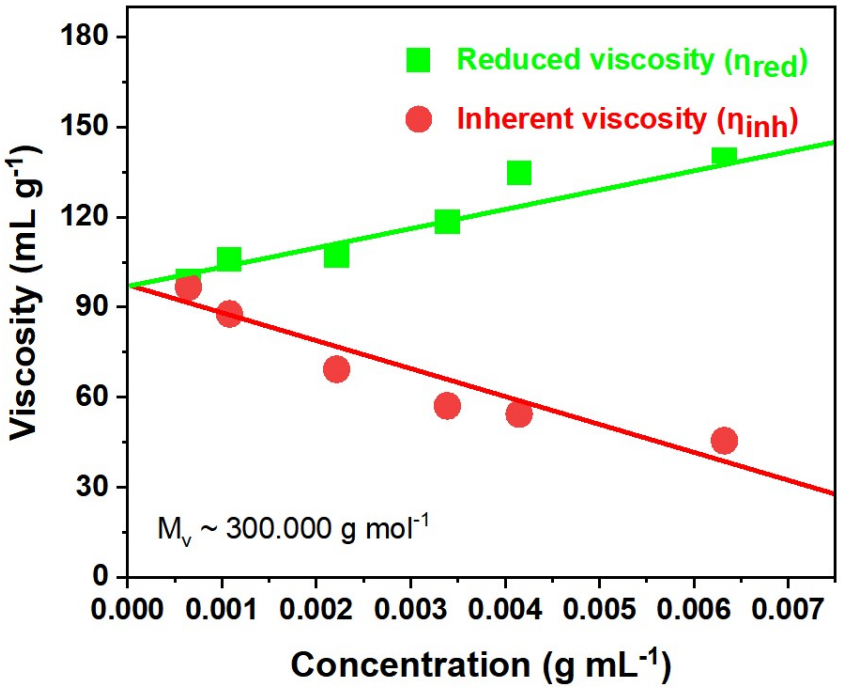

Figure S2. Viscosity of PBAPip-6-Br solution at different concentrations.

The intrinsic viscosity ([η]) of PBAPip-6-Br was determined using an Ubbelohde viscometer. The sample was dissolved in DMSO to obtain a homogeneous solution at different concentrations (c), and the efflux time (t_c) of each solution was recorded at 25 °C. The reduced (η_{red}) and inherent (η_{inh}) viscosities can be calculated using the following equations:

$$\eta_{red} = (t_c/t_0 - 1)/c \quad \text{(S-1)}$$

$$\eta_{inh} = (\ln t_c/t_0)/c \quad \text{(S-2)}$$

Here, t_0 is the efflux time for a DMSO solvent. In a plot of viscosity versus concentration, the intrinsic viscosity [η] was the y-intercept value obtained by extrapolating the η_{red} and η_{inh} to c = 0.

The M_v of PBAPip-6-Br was calculated by equation S-3:

$$[\eta] = k.\ M_v^a \quad \text{(S-3)}$$

Here, k = 0.03 and a = 0.75 are assumed for PBAPip-6-Br and DMSO combination.

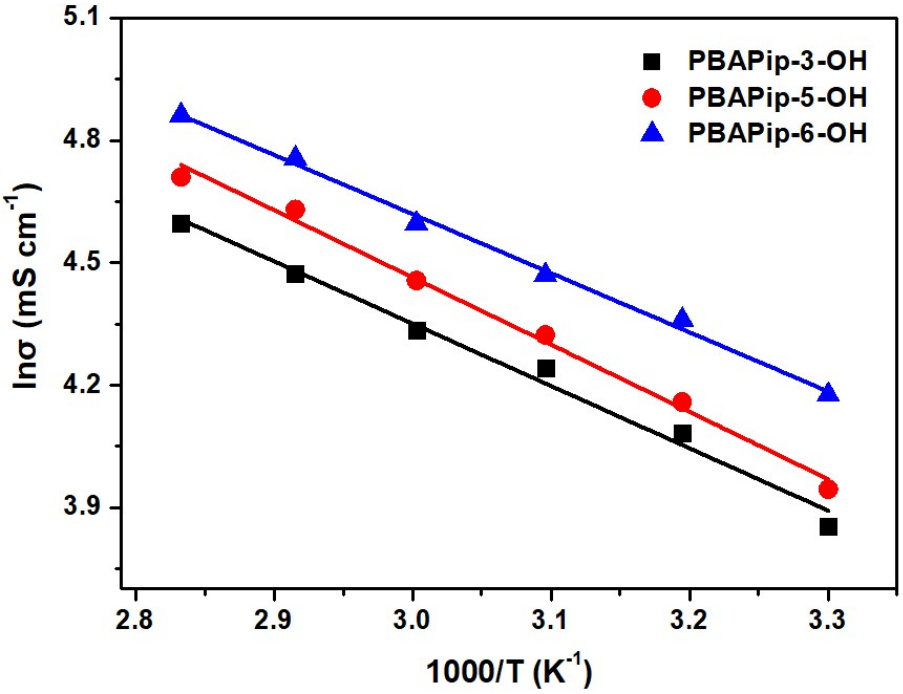

Figure S3. Arrhenius plots of the AEMs with different side chain lengths at various temperatures.

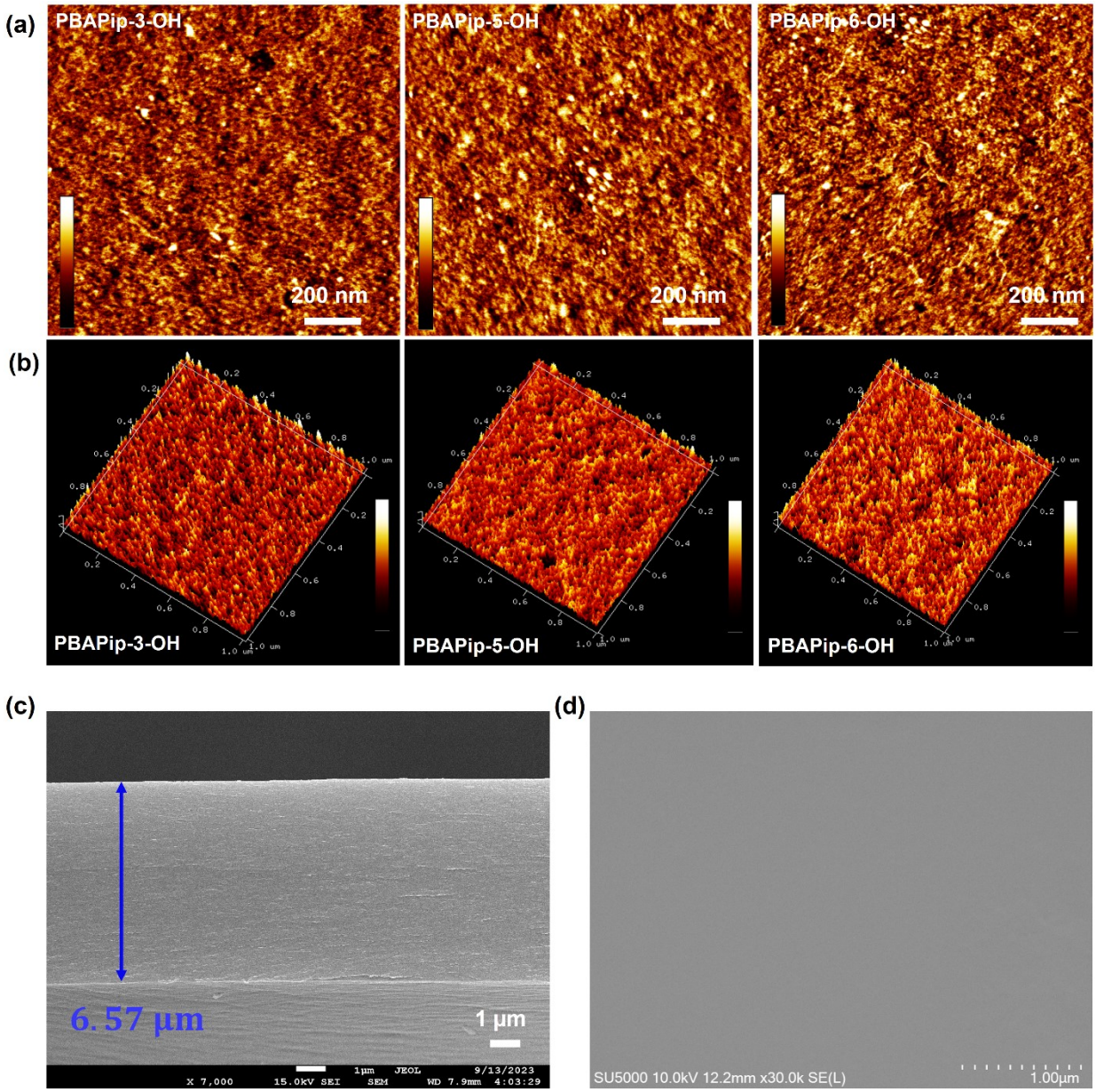

Figure S4. (a-b) Two- and three-dimensional AFM images of PBAPip-n-OH (n = 3, 5, and 6) membranes and (c-d) cross-sectional and surface SEM images of PBAPip-6-OH membrane.

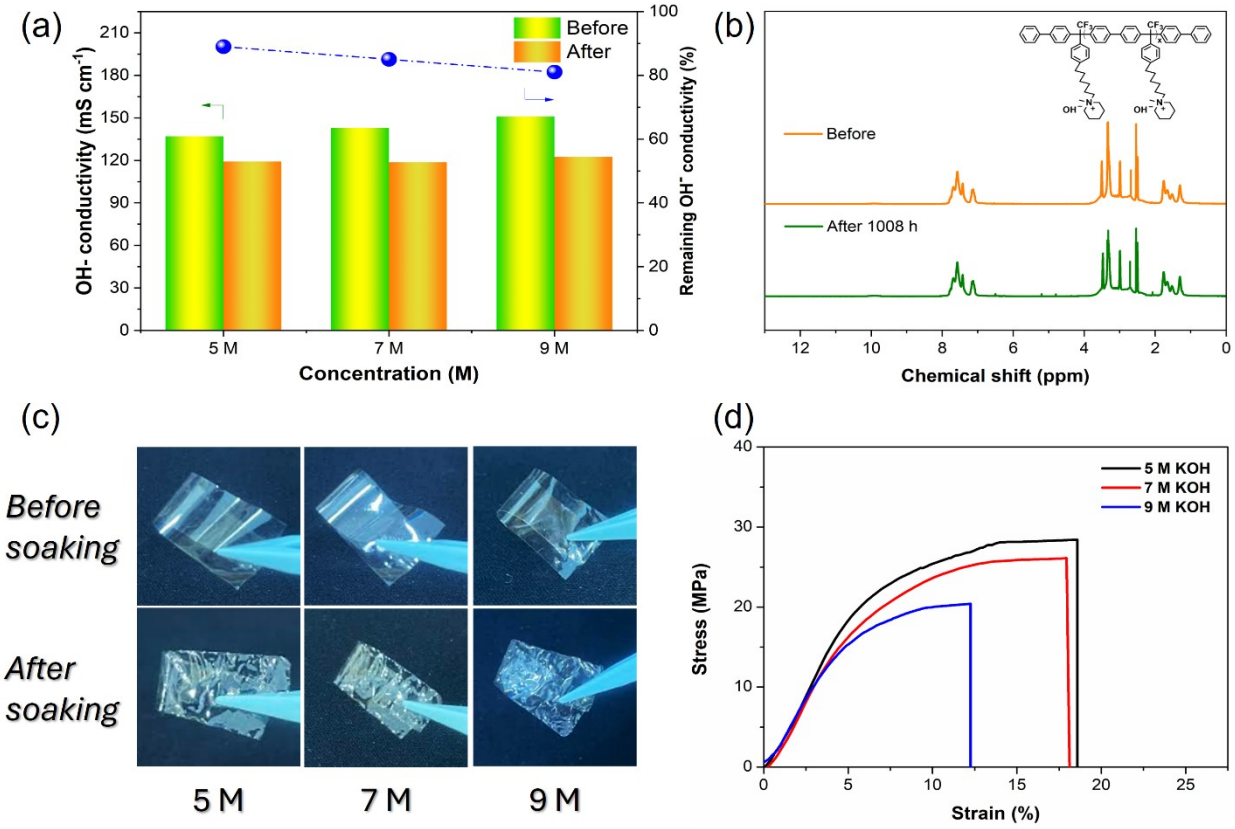

Figure S5. (a) Hydroxide conductivity of PBAPip-6-OH membrane before and after immersion in different KOH concentrations at 60 °C for 1008 h; (b) ^{1}H-NMR spectra of PBAPip-6-OH membrane before and after immersing in 5 M KOH solution at 60 °C for 1008 h; (c) visual images; and (d) the mechanical properties of PBAPip-6-OH membrane after soaking with different KOH concentrations for at 60 °C for 1008 h.

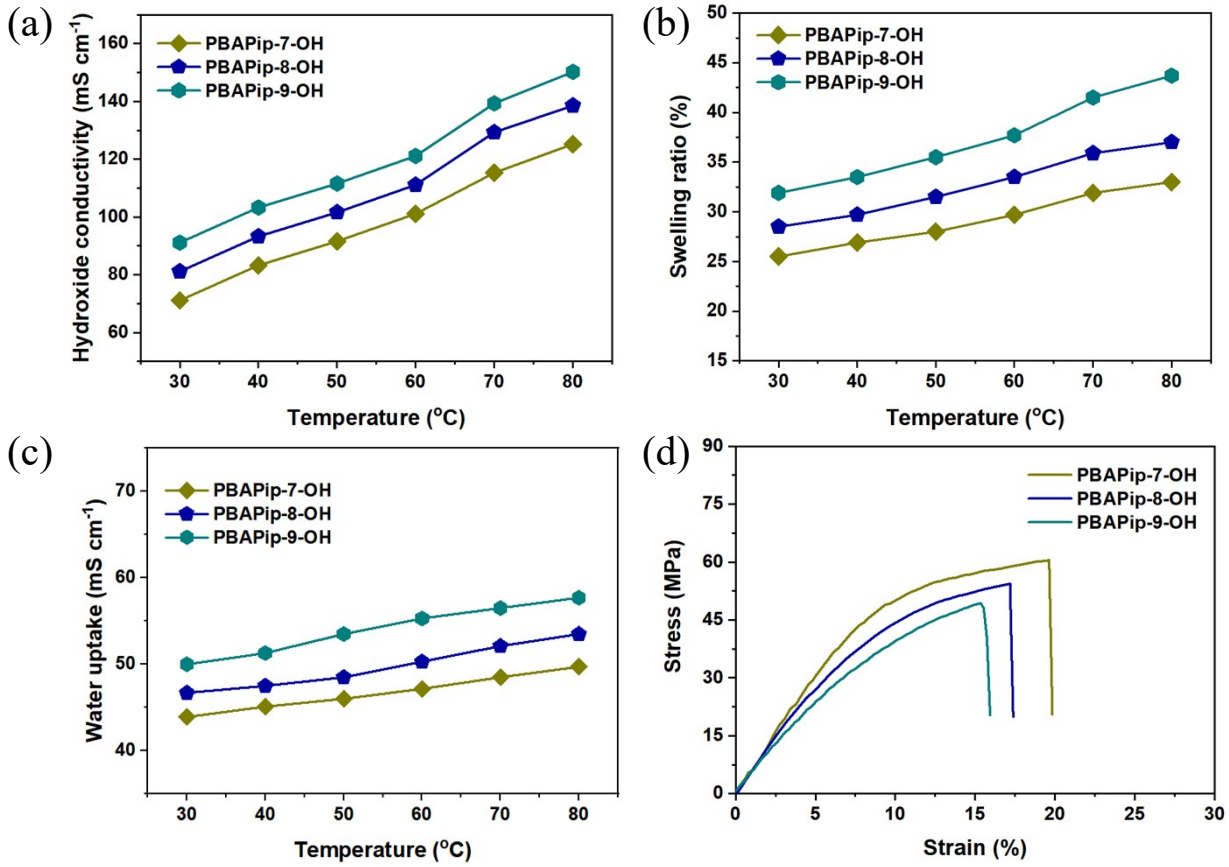

Figure S6. (a) Hydroxide ion conductivity; (b) swelling ratio; (c) water uptake; and (d) mechanical properties of PBAPip-n-Br membranes (n = 7, 8, and 9).

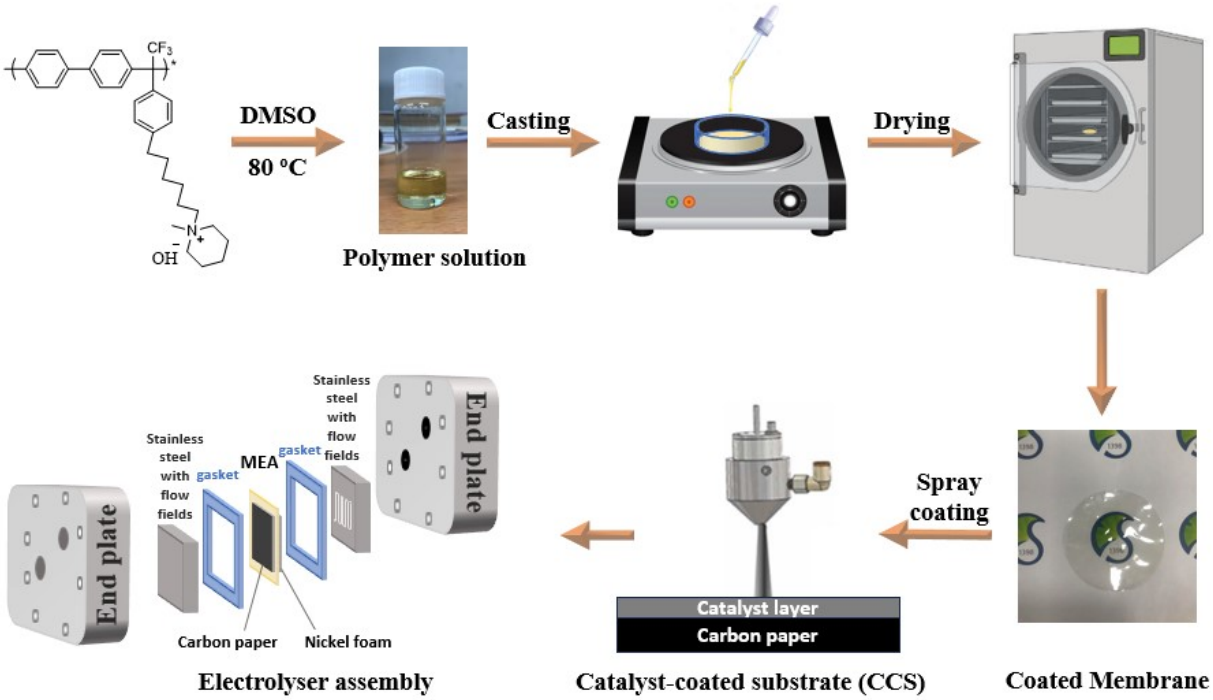

Figure S7. Preparation of anion exchange membranes, MEA, and the water electrolysis cell.

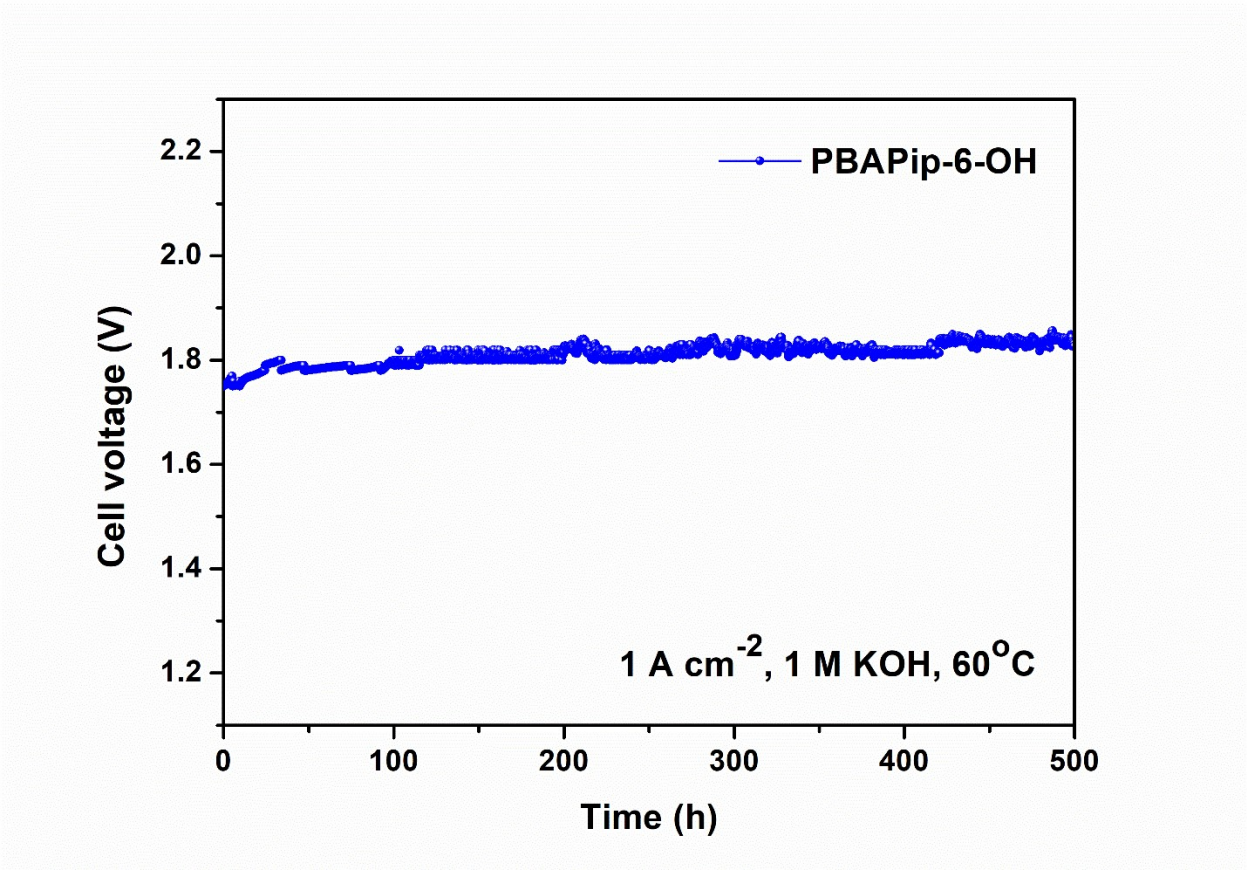

Figure S8. Long-term stability test of the PBAPip-6-OH-based AEMWE cell during 500 h.

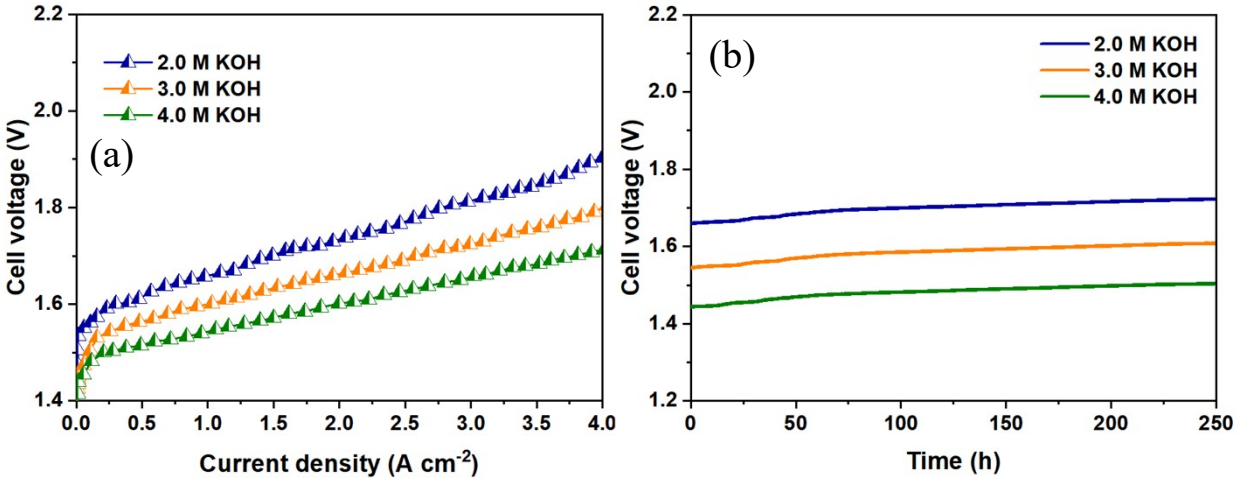

Figure S9. (a) Polarization curves at different KOH solution concentrations and (b) long-term stability test during 250 h at 1 A cm^{-2} of PBAPip-6-OH membrane.

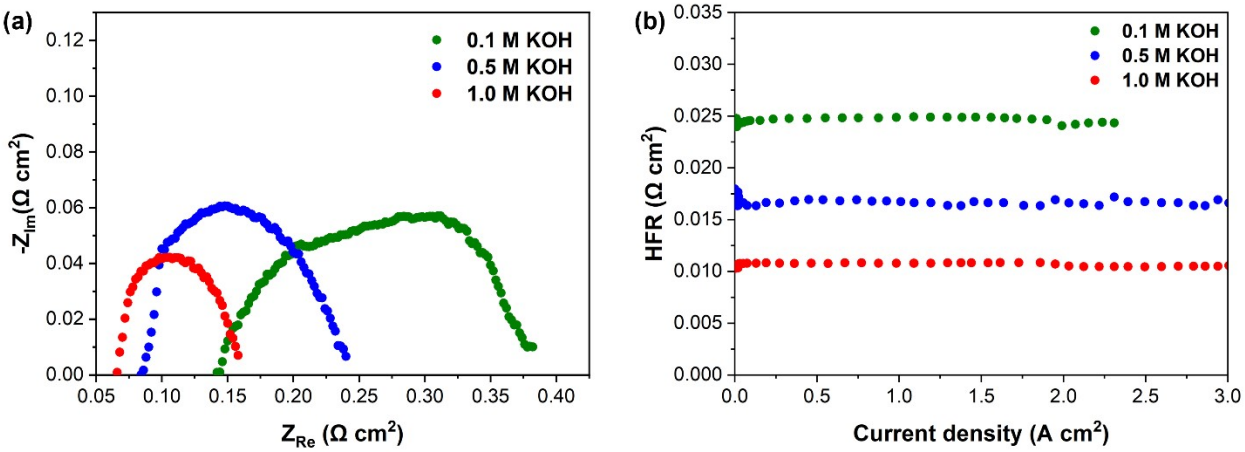

Figure S10. (a) Nyquist plot; and (b) HFR of AEMWE cells using PBAPip-6-OH membrane at various KOH concentrations.

Table S1: The degree of alkyl chain grafting and the quaternization level of N-methylpiperidine.

	I_{H_6}	I_a	I_p	η_g	η_q
PBAPip-3-Br	2.10	2.19	2.26	96%	97%
PBAPip-5-Br	2.32	2.41	2.55	95%	95%
PBAPip-6-Br	2.27	2.35	2.37	96%	97%

Here, I_{H_6}, I_a, and I_p are the intensity of the proton signals of the H_6, alkyl side chain, and piperidium functional groups, respectively. Besides, η_g and η_q are the degree of alkyl chain grafting and the quaternization level of N-methylpiperidine, respectively.

Table S2: Mechanical properties of the prepared AEMs at the dry states.

Samples	Tensile strength (MPa)	Elongation at break (%)	Young's modulus (GPa)
PBAPip-3-OH	52.5 ± 1.0	21.5 ± 0.4	1.18±0.0045
PBAPip-5-OH	60.1 ± 0.2	22.6 ± 0.7	1.00±0.0037
PBAPip-6-OH	67.5 ± 0.6	23.1 ± 0.3	0.96±0.0021

Table S3: The high-frequency resistance (HFR) and OH^- conductivity of the prepared membranes.

Concentration	HFR (Ω cm^2)	σ (mS cm^{-1})
0.1 M KOH	0.025	27.5
0.5 M KOH	0.017	39.3
1.0 M KOH	0.011	65.1

Here, the high-frequency resistance (HFR) of the anion exchange membranes can be determined using the following formula:

$$HFR\ (\Omega\ cm^2) = \frac{L}{\sigma \times A}$$

(S-4)

Where L is the thickness (cm), σ is the hydroxide conductivity, and A is the effective area (cm^2) of the prepared membranes.

Table S4: Comparison of cell performance between AEM fabricated in this study and other recently reported.

Membrane type	Anode	Cathode	Temp. (°C)	Feed	Current density (A cm^{-2})	Year	Ref.
PPO-ABCO	Ni foam	Ni foam	50	pure water	0.15	2014	[1,2]
Fumatech FAPQ	$NiFe_2O_4$	NiFeCo	60	1 M KOH	0.3	2017	[3]
PSF-ABCO	Ni/CP	Pt-Ni/CP	50	pure water	0.375	2017	[2]
PPO-TMA	Ni foam	Ni foam	50	pure water	0.6	2014	[1,2]
PSF-1M	Ni/CP	Pt-Ni/CP	50	pure water	0.6	2017	[2]
Aemion	$NiFe_2O_4$	NiFeCo	60	1 M KOH	0.63	2021	[4] 21
PSF-TMA	Ni/CP	Pt-Ni/CP	50	pure water	0.63	2017	[2] 51
FAA-3-50	*d*-Ni_3Fe_1	Pt/C	60	1 M KOH	0.75	2023	[4,5,6]
A-201	$NiFe_2O_4$	NiFeCo	60	1 M KOH	0.92	2021	[4]
PiperION	*d*-Ni_3Fe_1	Pt/C	50	1 M KOH	1.3	2023	[7]
Fumatech FAS-50	*d*-Ni_3Fe_1	Pt/C	60	1 M KOH	1.35	2023	[3]
AF1-HNN8-50-X	Ir black	Pt/C	50	1 M KOH	1.75	2020	[4]
FAA-3-PE-30	Ir black	Pt/C	50	1 M KOH	1.8	2019	[4]
FAA-3-PK-130	$Ce_{0.2}MnFe_{1.8}O_4$	Ni	50	1 M KOH	1.85	2019	[4]
Sustainion	*d*-Ni_3Fe_1	Pt/C	50	1 M KOH	2.2	2023	[3,4]

PVBC-MPy/35%PEK-cardo	NiFe-LDH/NF	MoNi/NF	60	1 M KOH	0.5	2019	[10]
L-ABPBI	*Ni foam*		70	3 M KOH	0.28	2016	[11]
C-ABPBI	*Ni foam*		70	3 M KOH	0.335	2016	[11]
This work	**Ni foam**	**Pt/C**	**60**	**1 M KOH**	**2.8**	**This work**	

Reference

1 J. Parrondo and V. Ramani, J. Electrochem. Soc., 2014, 161, F1015–F1020.

2 M. K. Cho, A. Lim, S. Y. Lee, H.-J. Kim, S. J. Yoo, Y.-E. Sung, H. S. Park and J. H. Jang, J. Electrochem. Sci. Technol, 2017, 8, 183–196.

3 Z. Liu, S. D. Sajjad, Y. Gao, H. Yang, J. J. Kaczur and R. I. Masel, International Journal of Hydrogen Energy, 2017, 42, 29661–29665.

4 D. Henkensmeier, M. Najibah, C. Harms, J. Žitka, J. Hnát and K. Bouzek, Journal of Electrochemical Energy Conversion and Storage, 2021, 18, 024001.

5 I. Gatto, A. Caprì, C. Lo Vecchio, S. Zignani, A. Patti and V. Baglio, International Journal of Hydrogen Energy, 2023, 48, 11914–11921.

6 J. E. Park, S. Y. Kang, S.-H. Oh, J. K. Kim, M. S. Lim, C.-Y. Ahn, Y.-H. Cho and Y.-E. Sung, Electrochimica Acta, 2019, 295, 99–106.

7 T.-H. Kong, P. Thangavel, S. Shin, S. Kwon, H. Choi, H. Lee, N. Park, J.-J. Woo and Y. Kwon, ACS Energy Lett., 2023, 8, 4666–4673.

8 T. Caielli, A. R. Ferrari, S. Bonizzoni, E. Sediva, A. Caprì, M. Santoro, I. Gatto, V. Baglio and P. Mustarelli, Journal of Power Sources, 2023, 557, 232532.

9 P. Fortin, T. Khoza, X. Cao, S. Y. Martinsen, A. Oyarce Barnett and S. Holdcroft, Journal of Power Sources, 2020, 451, 227814.

10 H. Li, M. R. Kraglund, A. K. Reumert, X. Ren, D. Aili and J. Yang, J. Mater. Chem. A, 2019, 7, 17914–17922.

11 L. A. Diaz, J. Hnát, N. Heredia, M. M. Bruno, F. A. Viva, M. Paidar, H. R. Corti, K. Bouzek and G. C. Abuin, Journal of Power Sources, 2016, 312, 128–136.